

Article

Effect of Smelting Time on Vanadium and Titanium Distribution Behavior and Slag Viscosity in HIs melt

Shushi Zhang ², Peng Hu ¹, Jiating Rao ¹, Zhenyang Wang ^{2,*}, Yanbing Zong ² and Jianliang Zhang ²

¹ State Key Laboratory of Comprehensive Utilization of Vanadium and Titanium Resources, Panzhihua 617000, China; hupeng000416@163.com (P.H.); raojiating416@163.com (J.R.)

² School of Metallurgical and Ecological Engineering, University of Science and Technology Beijing, Beijing 100083, China; zhangshushi416@163.com (S.Z.); zongyanbing416@163.com (Y.Z.); zhangjianliang416@163.com (J.Z.)

* Correspondence: wangzhenyang@ustb.edu.cn

Abstract: HIs melt is well suited for smelting vanadium–titanium magnetite due to its flexibility in feedstock selection and tolerance to high viscosity slag, compared with the blast furnace. In this work, the effect of smelting time on the distribution behavior and recovery rates of vanadium and titanium in HIs melt smelting of vanadium–titanium magnetite was investigated by experiment for the first time. The relationship between slag viscosity and temperature at different smelting times was further revealed by thermodynamic calculations. The experimental results show that extending the smelting time increases the FeO content in the slag, the L_V rose from 0.66 to 5.02, the L_{Ti} declined from 206.90 to 114.86, the shorter smelting time is favorable for increasing the recovery ratio of vanadium and titanium in metal and slag. In addition, slag viscosity decreases with increasing smelting time. The precipitation of high melting point titania spinel and $CaTiO_3$ phases is responsible for the significant increase in slag viscosity at 1300 °C.



Citation: Zhang, S.; Hu, P.; Rao, J.; Wang, Z.; Zong, Y.; Zhang, J. Effect of Smelting Time on Vanadium and Titanium Distribution Behavior and Slag Viscosity in HIs melt. *Metals* **2022**, *12*, 1019. <https://doi.org/10.3390/met12061019>

Academic Editors: Norman Toro, Edelmira Gálvez and Ricardo Jeldres

Received: 6 May 2022

Accepted: 11 June 2022

Published: 16 June 2022

Publisher's Note: MDPI stays neutral with regard to jurisdictional claims in published maps and institutional affiliations.



Copyright: © 2022 by the authors. Licensee MDPI, Basel, Switzerland. This article is an open access article distributed under the terms and conditions of the Creative Commons Attribution (CC BY) license (<https://creativecommons.org/licenses/by/4.0/>).

Keywords: HIs melt; vanadium titanomagnetite; distribution behavior; recovery; viscosity

1. Introduction

Vanadium–titanium magnetite is an important Fe, V, and Ti resource with a highly comprehensive utilization value [1–3]. Chinese vanadium–titanium magnetite reserves are plentiful but underutilized, with over 18 billion tons of proven vanadium and titanium magnetite reserves in China as of 2019 [4]. However, because of the complex phase structure and numerous mineral compositions, vanadium–titanium magnetite is classified as a typical polymetallic paragenetic resource that is difficult to treat and utilize [5–7]. Currently, the smelting process of vanadium–titanium magnetite is mainly a blast furnace–converter process [4,8]. However, it was found that the smelting operation and the comprehensive utilization of the V–Ti burden in the blast furnace were seriously affected by its poor tumbler strength compared with that of ordinary sintering [9–12]. In addition, the smelting atmosphere in the blast furnace is reductant, which promotes the over–reduction reaction of TiO_2 in the slag and the formation of Ti (C, N) with a high melting point, resulting in the increase of the slag viscosity and the decrease of the permeability in the blast furnace, which deteriorates the smelting conditions [13].

HIs melt is a molten reduction ironmaking process that has been used for the industrial smelting of ordinary iron ore [14,15]. The HIs melt process takes ore powder, flux, and coal powder as raw materials and has the advantage of less energy consumption and pollution compared with the blast furnace as it has no sintering and coking processes, which can avoid the adverse effects of vanadium and titanium magnetite sintering [16–18]. In addition, the atmosphere in the HIs melt smelting reduction furnace is weakly oxidizing, which could inhibit the over–reduction reaction of TiO_2 [18–20]. Moreover, the raw material is injected directly into the slag and metal through the lance in the HIs melt smelting reduction vessel,

it is not necessary to consider the gas permeability, thus HIs melt has twice the slag viscosity tolerance of the blast furnace [20–23].

In the blast furnace, the ore is gradually reduced to lose oxygen by the blast furnace gas during the slow downward movement and is eventually reduced to hot metal in the hearth, so it is not necessary to consider the effect of smelting time on production [24,25]. However, in the HIs melt smelting process, the raw material is reduced by carbon in the hot metal after being sprayed into the molten pool through the lance, thus the smelting time affects the production efficiency of HIs melt plants [23,26,27]. Since HIs melt smelting of vanadium–titanium magnetite has not yet been industrialized, it is essential to investigate the effect of smelting time on such a process.

In this paper, the effect of smelting time on the vanadium and titanium distribution behavior and slag viscosity properties in the HIs melt smelting of vanadium–titanium magnetite is investigated for the first time through experiments and thermodynamic calculations. First, melting pre-experiments and equilibrium experiments were designed to reveal the effect of smelting time on the vanadium and titanium distribution and recovery ratio. Then, the relationship between slag viscosity and temperature at different smelting times was calculated using the FactSage thermodynamic package. Finally, the phase and composition of the slag were analyzed by scanning electron microscopy equipped with energy dispersive spectroscopy. The results of this study could be helpful in promoting the industrialization of HIs melt smelting of vanadium–titanium magnetite.

2. Experimental Section

2.1. Materials

Vanadium–titanium magnetite was used in the experiments from Panzhihua, China. The mineralogical composition of the ore is shown in Table 1, the macroscopic morphology and particle size characteristics of the ore are shown in Figure 1.

Table 1. Composition of Panzhihua vanadium titanomagnetite (wt%).

Composition	Total Iron	SiO ₂	CaO	V ₂ O ₅	TiO ₂	MgO	Al ₂ O ₃	S	P
Content	56.03	2.98	0.89	0.62	10.87	2.84	2.83	0.61	0.01

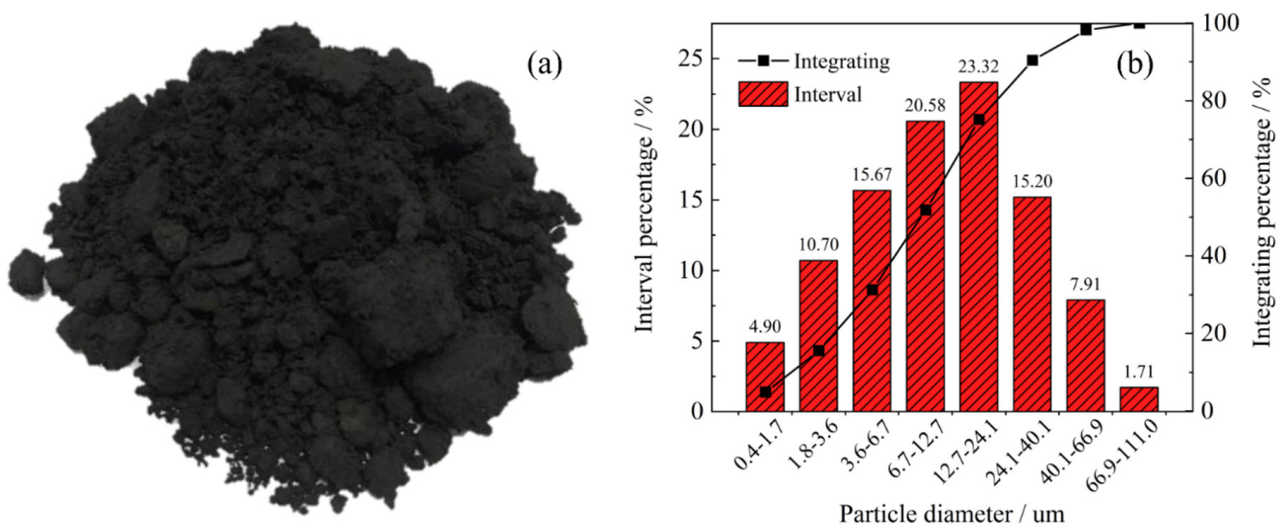


Figure 1. Macroscopic morphology and particle size characteristics of Panzhihua vanadium titanomagnetite. (a) Macroscopic morphology, (b) particle size distribution.

A simplified chemical composition of vanadium–titanium magnetite was used in experiments, experimental ore powders were synthesized using analytical grade chemical reagents. In order to avoid the influence of P and S elements on the experiment, the synthetic ore contained no P and S elements, while the binary basicity (CaO/SiO₂) was adjusted by

changing the CaO addition ratio to satisfy basicity of 1.2, which is the suitable basicity for smelting vanadium–titanium magnetite in HISMelt [13]. In addition, the graphite addition when the metal is carburized at 4% was calculated using the FactSage 8.1 thermodynamic package [28]. The proportions of raw ore, CaO, and graphite powder in the synthetic ore as well as the synthetic ore compositions that were normalized are shown in Table 2.

Table 2. Experimental ore powder composition.

Material Proportion (wt%)			Mineralogical Composition (wt%)							Graphite (g)
Raw Ore	CaO	Graphite	Total Iron	CaO	SiO ₂	Al ₂ O ₃	MgO	V ₂ O ₅	TiO ₂	
93.95	2.56	3.49	55.76	3.56	2.97	2.82	2.83	0.62	10.82	3.65

2.2. Synthetic Ore Samples

Experimental ore was synthesized using analytical grade chemical reagents to ensure the accuracy of the experimental results, the purity of reagents and their suppliers are shown in Table 3. Firstly, the experimental reagents such as CaO, SiO₂, Al₂O₃, MgO, and TiO₂ were roasted at 1000 °C for 2 h under argon protection, the CO₂ or H₂O likely present in the reagents were removed to reduce the experimental errors.

Table 3. Chemical reagent purity and their suppliers.

No.	Chemicals	Purity/%	Supplier
1	CaO	98	Sinopharm
2	SiO ₂	99	Sinopharm
3	Al ₂ O ₃	99	Sinopharm
4	MgO	98.5	Sinopharm
5	TiO ₂	98	Sinopharm
6	V ₂ O ₅	99	Energy
7	Fe	98	Aladdin
8	Graphite	99.9	Macklin

2.3. Experimental Scheme and Procedure

The experiments were divided into melting pre-experiments and equilibrium experiments. As shown in Figure 2, the purpose of the melting pre-experiment was to obtain the melting time of synthetic ore at 1500 °C (the melting time corresponds to the heating time during the melting stage in the equilibrium experiments). The equilibrium experiment was divided into the melting stage and the equilibrium stage. In the melting stage, the synthetic ore was melted at high temperature and the slag–metal started to separate, the melting stage time was the ore melting time in the melting pre-experiment. In the equilibrium stage, the separation of slag and metal was completed, and the element distribution in slag and metal gradually reached equilibrium.

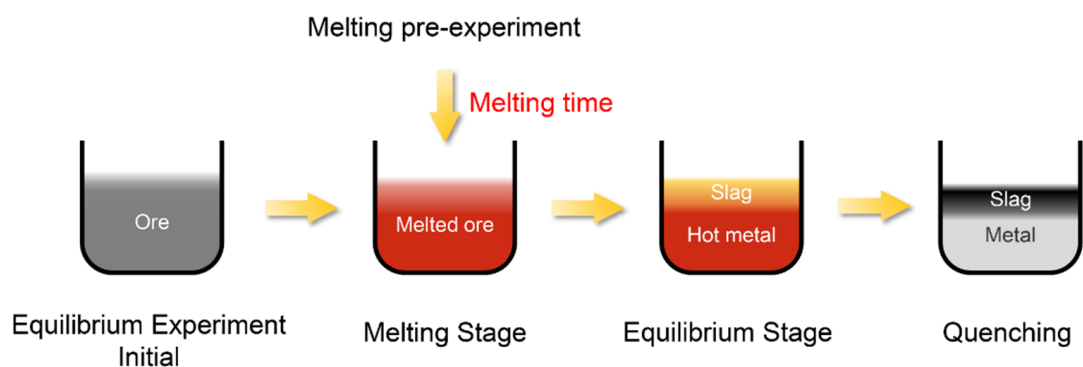


Figure 2. Schematic diagram of the experimental procedure.

2.3.1. Melting Pre-Experiments

The chemical reagents were weighed and mixed thoroughly according to the synthetic ore composition, 0.8 g of synthetic ore was added to the powder briquetting machine, and a cylindrical material block with a diameter of 8 mm and a height of 4 mm was obtained after being kept under 5 Mpa pressure for 1 min, as shown in Figure 3.

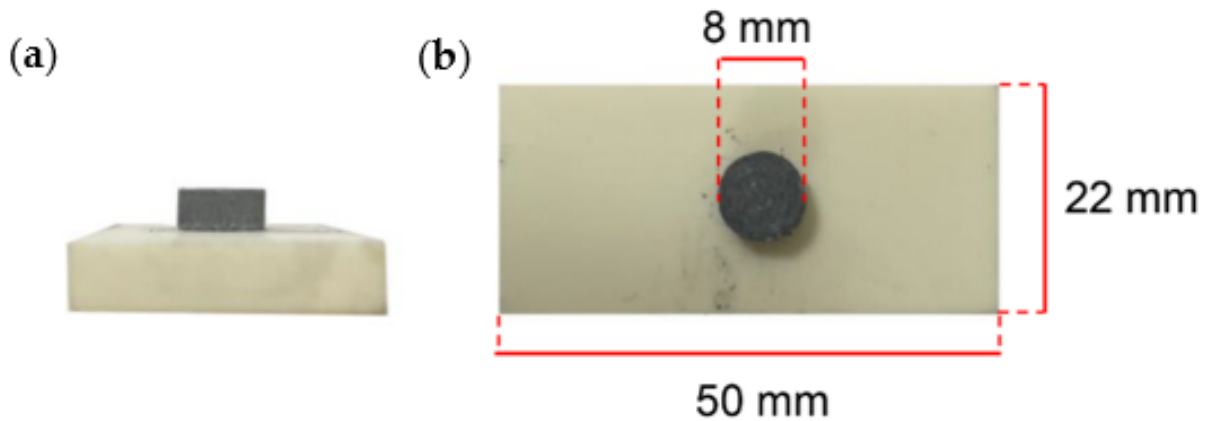


Figure 3. Macroscopic morphology of cylindrical material block. (a) Front view, (b) top view.

Then, the cylindrical material block was placed on an Al_2O_3 sheet ($50 \times 22 \times 6$ mm) inside a graphite boat, then the graphite boat was put into the ash fusibility tester (abbreviated as AFT; Chang Sha U-Therm Instrument Manufacturing Co., Ltd.; Model YH-HRD 3000, Changsha, Hunan, China). The AFT was sealed and then argon (99.999%, 3 L/min) was injected, the cylindrical material block was heated (at a rate of $500^\circ\text{C}/\text{h}$) to 1500°C and then kept at constant temperature. The pictures were taken and recorded every 10 s. Finally, the melting time of the ore was determined by comparing the deformation and angle of the columnar blocks at 1500°C with Photoshop graphic processing software (2020, Adobe, San Jose, CA, USA).

2.3.2. Equilibrium Experiments

The weighed Fe, V_2O_5 , and graphite powders were thoroughly mixed and denominated as sample 1, and CaO, SiO_2 , Al_2O_3 , MgO, and TiO_2 were mixed and labeled as sample 2. Sample 1 was placed at the bottom of the MgO crucible with 18 mm inner diameter and 50 mm height, sample 2 was covered on sample 1. With this method, the melting process of the synthetic ore was accelerated and the equilibrium process was promoted. Finally, the MgO crucible was placed in the constant temperature zone inside the Al_2O_3 casing of the elevated temperature tubular furnace. Figure 4 shows a schematic diagram of the elevated temperature vertical tubular furnace.

The synthetic ore was heated to 1500°C at a heating rate of $300^\circ\text{C}/\text{h}$ under the protection of argon (3 L/min) and then maintained at constant temperature. The equilibrium experiment entered the melting stage, the melting stage time is the synthetic ore melting time in the melting pre-experiment.

Then the equilibrium experiment entered the equilibrium stage, and the argon flow rate was quickly adjusted to 1 L/min and kept at a constant temperature for 1 h, 2 h and 3 h. The 1 h, 2 h, and 3 h slag and metal samples were rapidly removed and quenched using argon (99.999%) purging. The heating process for the melting and equilibrium experiment is shown in Figure 5.

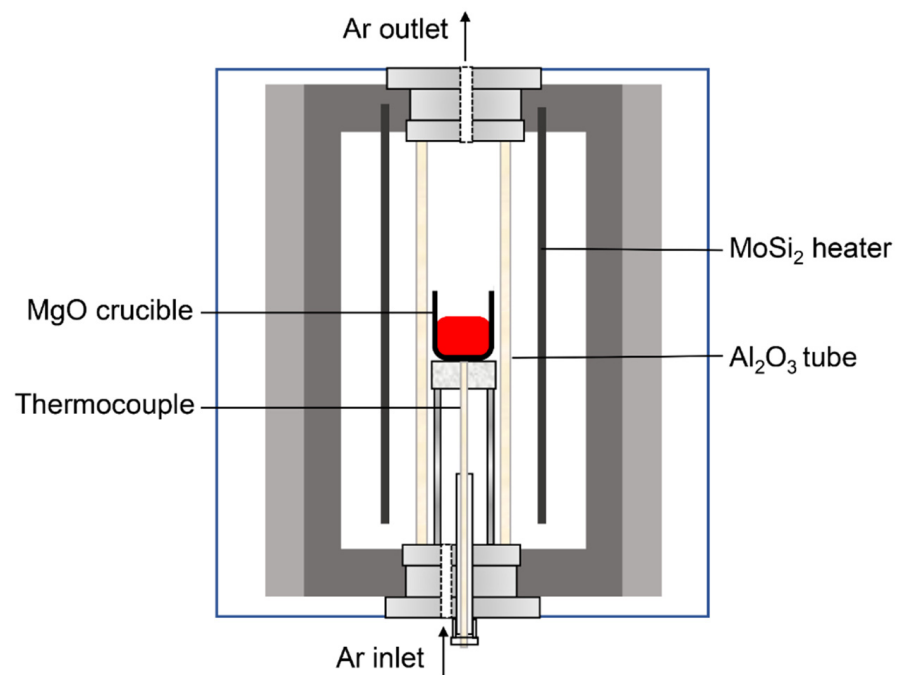


Figure 4. Structural diagram of elevated temperature vertical tubular furnace.

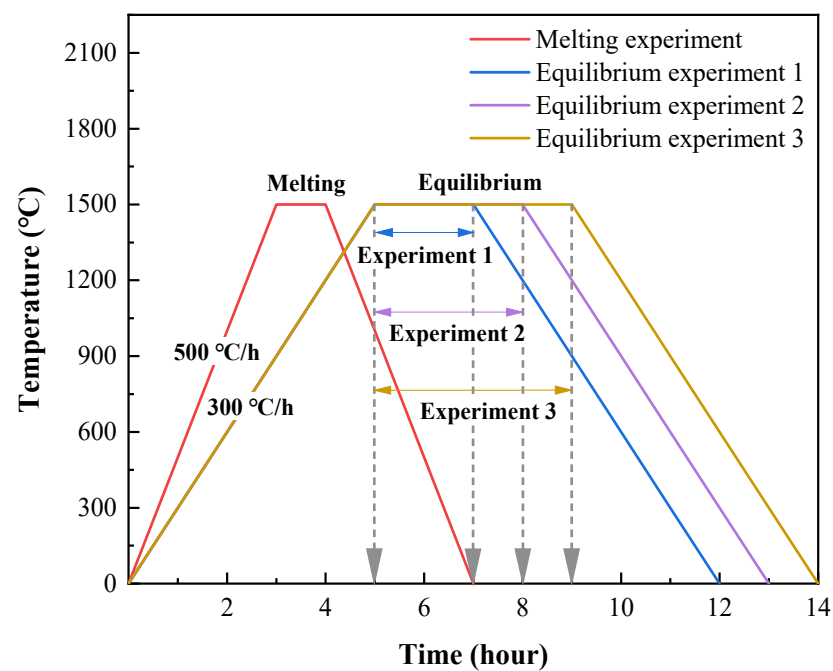


Figure 5. Heating process of melting and equilibrium experiment.

3. Results and Discussion

3.1. Ore Melting Behavior

Figure 6 shows a photograph of the melting process for the cylindrical material block. As shown in Figure 6, it can be observed that the shape of the column block in the initial state was complete, and the contact angle between column block and the Al_2O_3 sheet was 90° . When the AFT was heated up to 1500°C , the column block had obvious melting and deformation, the contact angle between the column block and the Al_2O_3 sheet decreased, but still remained between $80\text{--}90^\circ$. When the column block was heated at 1500°C for 50 min, the contact angle between the column block and the Al_2O_3 sheet was reduced to about 70° , and the column block was completely melted into liquid droplets. Therefore,

the column block was completely melted after being kept at 1500 °C for 50 min. To ensure that the synthetic ore was completely melted, finally, the melting time was determined to be 60 min.

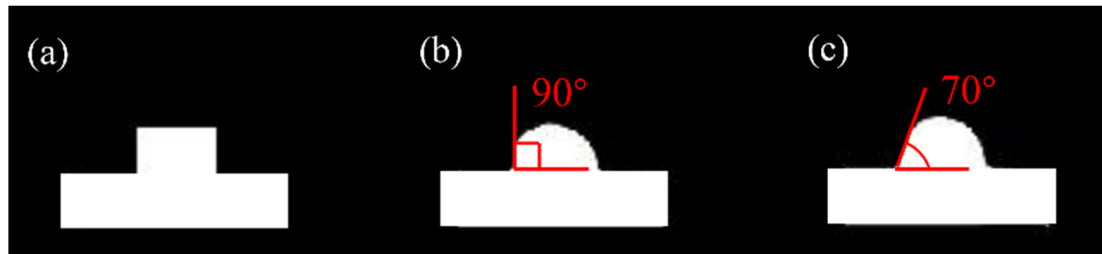


Figure 6. Melting process of column material block. (a) Sample at 25 °C, (b) sample at 1500 °C for 0 min, (c) sample at 1500 °C for 50 min.

3.2. Effect of Smelting Time on Element Distribution Behavior and Recovery

Table 4 shows the composition of slag and metal at different smelting times detected by SEM–EDS. The content of FeO, V₂O₃, and TiO₂ in the slag increased as the smelting time was extended, which was because the atmosphere of the HIs melt SRV furnace is weakly oxidizing, and more Fe, V, and Ti elements in the hot metal are oxidized into the slag with a longer smelting time. With the increase in smelting time, the V content in the hot metal was reduced, which was consistent with the above findings.

Table 4. Composition of slag and metal at different smelting times.

Smelting Time	Slag (wt%)						Hot Metal (wt%)			
	FeO	CaO	MgO	Al ₂ O ₃	SiO ₂	V ₂ O ₃	TiO ₂	Si	Ti	V
1 h	1.86	16.77	13.33	11.05	19.20	0.53	37.24	0.07	0.18	0.81
2 h	2.71	15.55	12.36	10.16	17.53	1.59	40.10	0.14	0.31	0.53
3 h	2.93	15.55	12.37	9.94	16.05	1.81	41.35	0.36	0.36	0.36

The elemental distribution ratios were defined as follows:

$$L_M = \frac{w_{(MO_x)}}{w_{[M]}} \quad (1)$$

where M is the V and Ti elements, $w_{[M]}$ and $w_{(MO_x)}$ are the mass fraction of the element M in metal and M oxides in slag individually, the L_M is the distribution ratio of element M.

Figure 7 shows the change of vanadium and titanium distribution ratios (L_V , L_{Ti}) with smelting time. As the smelting time was extended from 1 to 3 h, the L_V rose from 0.66 to 5.02 and L_{Ti} declined from 206.90 to 114.86. The reason for this is that extending the smelting time increases the FeO content in the slag under a weakly oxidizing atmosphere, element V is oxidized to V₂O₃ by FeO. However, at the current FeO content, the restrictive step of titanium distribution behavior was the smelting time rather than the oxygen potential, therefore, the titanium distribution ratio decreased with increasing smelting time.

The elemental recovery ratios were defined as follows

$$\varepsilon_V = \frac{m_{V \text{ metal}}}{m_{V \text{ metal}} + m_{V \text{ slag}}} \quad (2)$$

$$\varepsilon_{Ti} = \frac{m_{Ti \text{ slag}}}{m_{Ti \text{ metal}} + m_{Ti \text{ slag}}} \quad (3)$$

where $m_{V \text{ metal}}$ and $m_{Ti \text{ metal}}$ are the mass of V and Ti in the metal, $m_{V \text{ slag}}$ and $m_{Ti \text{ slag}}$ are the mass of V and Ti in the slag individually, the ε_V and ε_{Ti} are the recovery ratio of V and Ti.

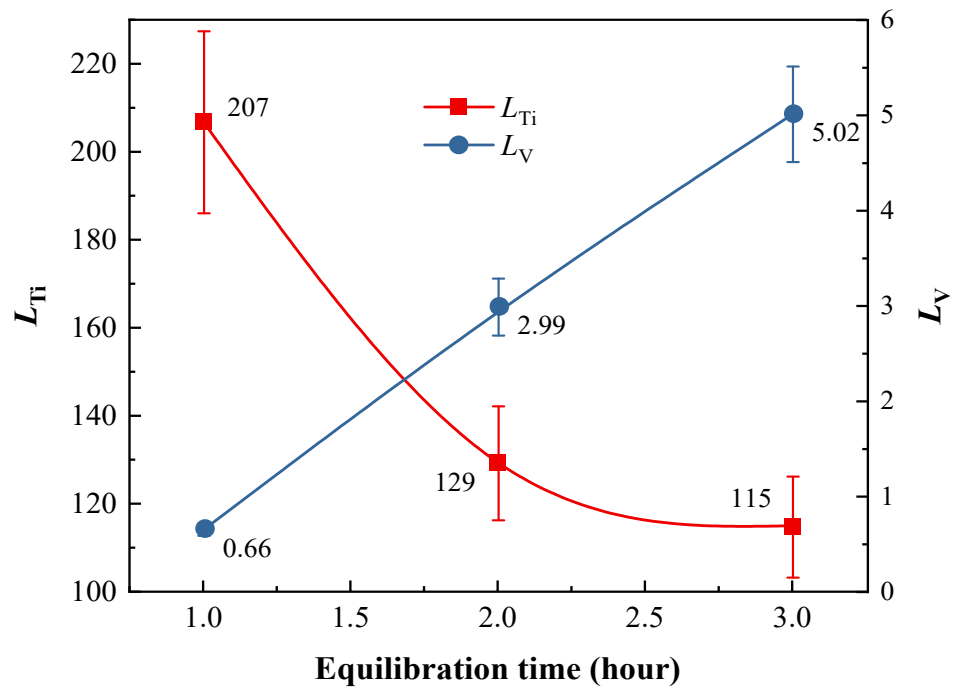


Figure 7. Effect of smelting time on vanadium and titanium distribution ratio.

In order to obtain more valuable data for industrial production, the effect of smelting time on the recovery of vanadium and titanium (ϵ_V , ϵ_{Ti}) was investigated. As shown in Figure 8, both ϵ_V and ϵ_{Ti} were reduced with a longer smelting time. Therefore, there is no doubt that the shorter smelting time is favorable to increase the recovery ratio of vanadium in hot metal and titanium in slag. Currently, according to actual production data from a Chinese blast furnace for vanadium and titanium magnetite smelting, the vanadium recovery is 74.3% and the titanium recovery is 95.4%. As a result, under the current research conditions, HIs melt has higher vanadium and titanium recoveries than the blast furnace.

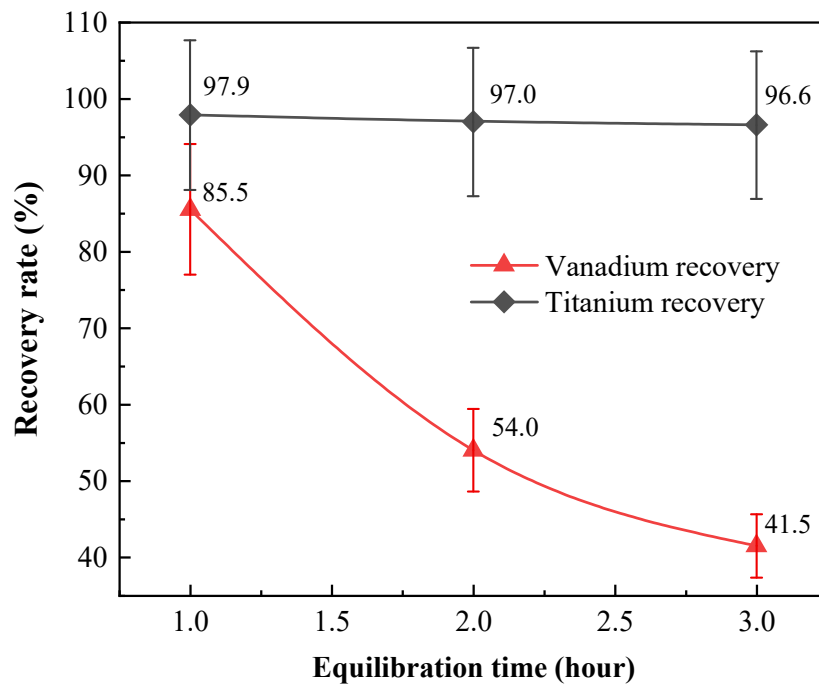


Figure 8. Effect of smelting time on the recovery of vanadium and titanium.

3.3. Effect of Smelting Time on Slag Viscosity Properties

The ironmaking process is also a slag refining process, and the slag properties are critical to the process of HIs melt smelting of vanadium–titanium magnetite. As a result, the changes in slag viscosity with temperature at different smelting times were calculated using FactSage, and the slag viscosity was corrected using the Einstein–Roscoe Equation, as shown in Equation (4).

$$\eta_{\text{solid+liquid}} \approx \eta_{\text{liquid}} \cdot (1 - \text{solid fraction})^{-2.5} \quad (4)$$

where η_{liquid} is the viscosity of liquid slag, $\eta_{\text{solid+liquid}}$ is the viscosity for solid–liquid mixed slag. The original Einstein–Roscoe equation used ‘volume fraction of solid’ instead of ‘solid fraction’ and a correction term for morphology; we can simply use the solid fraction (wt%) for this equation as an approximation.

Figure 9 demonstrates that the slag viscosity reduced with increasing smelting temperature at different smelting times, and the appearance of the inflection point showed a clear basic slag characteristic. The inflection point in the figure was about 1300 °C. However, as the smelting time was extended, the slag viscosity showed a tendency to decline, although the tendency was weak. It could be explained by the fact that the smelting time promotes the increase of FeO content in the slag, FeO has the basic oxide properties that could depolymerize the Al–O and Si–O tetrahedral structure in the slag, resulting in the reduction of slag viscosity [29–31].

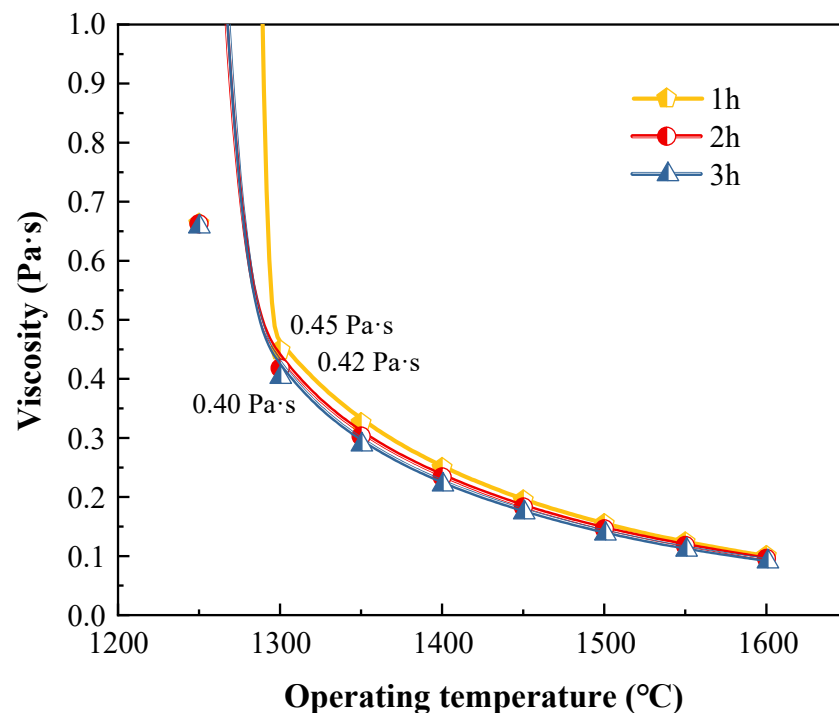


Figure 9. Effect of smelting time on slag viscosity.

Figure 10 shows the microscopic morphology and phases of slag with a smelting time of 3 h. As shown in the red box in Figure 10a,b, the main phase in the slag was the rod-like CaTiO_3 phase. As shown in Figure 10c, the titania spinel and CaTiO_3 phases started to precipitate from liquid slag when the temperature dropped below 1300 °C. As a result, the significant increase in slag viscosity at 1300 °C in Figure 9 could be attributed to the precipitation of the high melting point CaTiO_3 phase from the liquid slag.

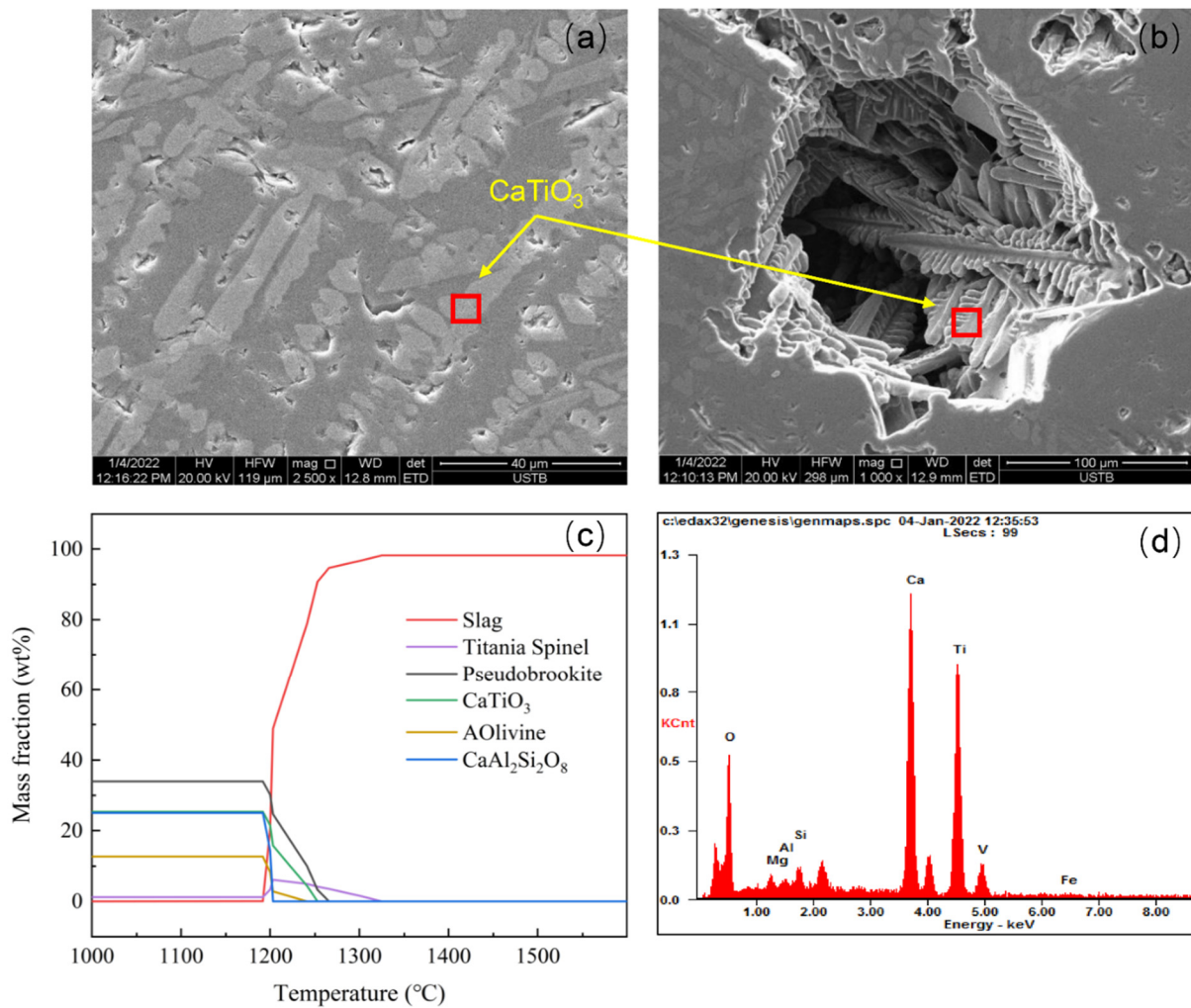


Figure 10. (a) Microscopic morphology and physical phases of slag with smelting time of 3 h, (b) SEM image of the high titanium slag, (c) changes in the solid phase precipitation during equilibrium cooling of the slag as calculated using the Factsage software, (d) EDS spectrum obtained for the CaTiO_3 inclusions shown in (b).

4. Conclusions

In this paper, the effect of smelting time on element distribution and slag viscosity properties when smelting vanadium–titanium magnetite in HIsmelt was investigated by experimental and thermodynamic calculations.

(1) Extending the smelting time increases the FeO content in the slag, element V is oxidized to V_2O_3 by FeO, the L_V rose from 0.66 to 5.02. However, at the current FeO content, the restrictive step of titanium distribution behavior is the smelting time rather than the oxygen potential, the L_{Ti} declined from 206.90 to 114.86. The shorter smelting time is favorable for increasing the recovery ratio of vanadium and titanium in the metal and slag.

(2) As the smelting time is extended, FeO depolymerizes the Al–O and Si–O tetrahedral structure in the slag, resulting in the reduction of the slag viscosity. The precipitation of high melting point titania spinel and CaTiO_3 phases is responsible for the significant increase in slag viscosity at 1300 °C.

Author Contributions: Conceptualization, Z.W., P.H. and J.R.; methodology, Z.W. and S.Z.; software, S.Z.; validation, J.Z., Y.Z. and Z.W.; formal analysis, S.Z.; investigation, S.Z.; resources, P.H. and J.R.; data curation, S.Z.; writing—original draft preparation, S.Z.; writing—review and editing, S.Z.;

visualization, Z.W. and S.Z.; supervision, J.Z. and Y.Z.; project administration, P.H. and J.R.; funding acquisition, Z.W. All authors have read and agreed to the published version of the manuscript.

Funding: This research was funded by the State Key Laboratory of Vanadium and Titanium Resources Comprehensive Utilization, Project No.: 2020P4FZG06A, and the China Postdoctoral Science Foundation, Project No.: BX20200045 and 2021M690370.

Institutional Review Board Statement: Not applicable.

Informed Consent Statement: Not applicable.

Conflicts of Interest: The authors declare no conflict of interest.

References

1. Tang, W.D.; Xue, X.X.; Yang, S.T.; Zhang, L.H.; Huang, Z. Influence of basicity and temperature on bonding phase strength, microstructure, and mineralogy of high-chromium vanadium–titanium magnetite. *Int. J. Miner. Metall. Mater.* **2018**, *25*, 871–880. [[CrossRef](#)]
2. Zhou, M.; Jiang, T.; Ding, X.; Ma, S.; Wei, G.; Xue, X. Thermodynamic study of direct reduction of high-chromium vanadium–titanium magnetite (HCVTM) based on phase equilibrium calculation model. *J. Therm. Anal. Calorim.* **2019**, *136*, 885–892. [[CrossRef](#)]
3. Xu, C.; Zhang, Y.; Liu, T.; Huang, J. Characterization and Pre-Concentration of Low-Grade Vanadium–Titanium Magnetite Ore. *Minerals* **2017**, *7*, 137. [[CrossRef](#)]
4. Zhang, S.; Hu, P.; Rao, J.; Wang, Z.; Zhang, J.; Zong, Y. Comprehensive utilization status of vanadium–titanium magnetite and feasibility analysis of HIs melt smelting. *J. Cent. South Univ. (Sci. Technol.)* **2021**, *52*, 3085–3092.
5. Zhou, M.; Jiang, T.; Yang, S.; Xue, X. Vanadium–titanium magnetite ore blend optimization for sinter strength based on iron ore basic sintering characteristics. *Int. J. Miner. Processing* **2015**, *142*, 125–133. [[CrossRef](#)]
6. Feng, C.; Chu, M.; Tang, J.; Tang, Y.; Liu, Z. Main metallurgical performance and phases for different types of titanium-bearing blast furnace slags. *J. Cent. South Univ. (Sci. Technol.)* **2016**, *47*, 2556–2562.
7. Chang, F.; Zhao, B.; Li, L.; Geng, L.; Zhang, Z. Research status and prospect of vanadium extraction technology from vanadium–titanium magnetite. *Iron Steel Vanadium Titan.* **2018**, *39*, 71–78.
8. Sun, H.; Zhu, Q.; Li, H. The technical state and development trend of the direct reduction of titanomagnetite by fluidized bed. *Chin. J. Process Eng.* **2018**, *18*, 1146–1159.
9. Zigu, H.; Hongcai, F.; Lian, L.; Turner, S. Comprehensive Utilization of Vanadium–Titanium Magnetite Deposits in China Has Come to a New Level. *Acta Geol. Sin.–Engl. Ed.* **2013**, *87*, 286–287. [[CrossRef](#)]
10. Chen, S.Y.; Chu, M.S. Metalizing reduction and magnetic separation of vanadium titanomagnetite based on hot briquetting. *Int. J. Miner. Metall. Mater.* **2014**, *21*, 225–233. [[CrossRef](#)]
11. Zhao, L.; Wang, L.; Qi, T.; Chen, D.; Zhao, H.; Liu, Y. A novel method to extract iron, titanium, vanadium, and chromium from high-chromium vanadium-bearing titanomagnetite concentrates. *Hydrometallurgy* **2014**, *149*, 106–109. [[CrossRef](#)]
12. Zhang, Y.M.; Wang, L.N.; Chen, D.S.; Wang, W.J.; Liu, Y.H.; Zhao, H.X.; Qi, T. A method for recovery of iron, titanium, and vanadium from vanadium-bearing titanomagnetite. *Int. J. Miner. Metall. Mater.* **2018**, *25*, 131–144. [[CrossRef](#)]
13. Zhang, S.; Wang, Z.; Hu, P.; Rao, J.; Zhang, J.; Pang, J. HIs melt smelting vanadium titanomagnetite: The effect of composition and temperature on the distribution behavior of V, Ti, and Si and the feasibility of smelting vanadium titanomagnetite with natural basicity. *Trans. Nonferrous Met. Soc. China* **2022**. [[CrossRef](#)]
14. Zhang, J.; Li, K.; Zhang, G.; Wang, Z.; Zhang, X. Technological Innovation and Latest Production Index of HIs melt Process in Shandong Molong. *Ironmaking* **2018**, *37*, 56–60.
15. Zhang, J.; Zhang, G.; Liu, Z.; Wang, Z.; Li, K.; Zhang, X. The production operation and main characteristics of HIs melt process in Shandong Molong. *China Metall.* **2018**, *28*, 37–41.
16. Ma, H.; Jiao, K.; Zhang, J. The influence of basicity and TiO₂ on the crystallization behavior of high Ti-bearing slags. *CrystEngComm* **2019**, *22*, 361–370. [[CrossRef](#)]
17. Kurunov, I.F. The direct production of iron and alternatives to the blast furnace in iron metallurgy for the 21st century. *Metallurgist* **2010**, *54*, 335–342. [[CrossRef](#)]
18. Schenk, J.L. Recent status of fluidized bed technologies for producing iron input materials for steelmaking. *Particuology* **2011**, *9*, 14–23. [[CrossRef](#)]
19. Li, Y.; Li, Y.; Fruehan, R.J. Formation of Titanium Carbonitride from Hot Metal. *ISIJ Int.* **2001**, *41*, 6. [[CrossRef](#)]
20. Stephens, D.; Tabib, M.; Schwarz, M.P.; Davis, M. CFD simulation of bath dynamics in the HIs melt smelt reduction vessel for iron production. *Prog. Comput. Fluid Dyn. Int. J.* **2012**, *12*, 196. [[CrossRef](#)]
21. Neil, G.; Rod, D.; Wang, D. HIs melt ironmaking process. *World Steel* **2010**, *10*, 1–5.
22. Kitagawa, T. Present Status of the Development of Smelting Reduction Technologies. *Tetsu-to-Hagane* **2002**, *88*, 430–443. [[CrossRef](#)]
23. Jacques, P. HIs melt technology suitable for vanadium–titanium magnetite. In Proceedings of the 2010 Annual Conference of Non-Blast Furnace Ironmaking and Seminar on Comprehensive Utilization of Vanadium–titanium Magnetite, Panzhihua, China, 27–29 October 2010; The Chinese Society for Metals 2010. pp. 233–238.

24. Chu, M.; Tang, J.; Liu, Z.; Ying, Z. Present situation and progress of comprehensive utilization for high-chromium vanadium-bearing titanomagnetite. *J. Iron Steel Res.* **2017**, *29*, 335–344.
25. Li, R.; Liu, T.; Zhang, Y.; Huang, J.; Xu, C. Efficient Extraction of Vanadium from Vanadium–Titanium Magnetite Concentrate by Potassium Salt Roasting Additives. *Minerals* **2018**, *8*, 25. [[CrossRef](#)]
26. Wang, M.; Ren, R.; Dong, H.; Zhang, G.; Liu, S. Latest technology of melting reduction ironmaking process and discussion of process route choice. *Iron Steel* **2020**, *55*, 145–150.
27. Li, Y.-L.; Li, H.-B.; Wang, H.; Qing, S.; Hu, J.-H.; Hou, Y.-L.; Li, H.; Li, L.-Q. Smelting potential of HIs melt technology for high-phosphorus iron ore and ilmenite. In Proceedings of the 2011 International Conference on Computer Distributed Control and Intelligent Environmental Monitoring, Changsha, China, 19–20 February 2011; pp. 1283–1286.
28. Bale, C.W.; Bélisle, E.; Chartrand, P.; Decterov, S.A.; Eriksson, G.; Gheribi, A.E.; Hack, K.; Jung, I.H.; Kang, Y.B.; Melançon, J.; et al. Reprint of: FactSage thermochemical software and databases, 2010–2016. *Calphad* **2016**, *55*, 1–19. [[CrossRef](#)]
29. Ma, S.; Li, K.; Zhang, J.; Jiang, C.; Sun, M.; Li, H.; Wang, Z.; Bi, Z. Structural Characteristics of CaO–SiO₂–Al₂O₃–FeO Slag with Various FeO Contents Based on Molecular Dynamics Simulations. *JOM* **2021**, *73*, 1637–1645. [[CrossRef](#)]
30. Ma, H.; Jiao, K.; Zhang, J.; Zong, Y.; Zhang, J.; Meng, S. Viscosity of CaO–MgO–Al₂O₃–SiO₂–TiO₂–FeO slag with varying TiO₂ content: The Effect of Crystallization on Viscosity Abrupt Behavior. *Ceram. Int.* **2021**, *47*, 17445–17454. [[CrossRef](#)]
31. Ma, J.; Fu, G.Q.; Li, W.; Zhu, M.Y. Influence of TiO₂ on the melting property and viscosity of Cr-containing high-Ti melting slag. *Int. J. Miner. Metall. Mater.* **2020**, *27*, 310–318. [[CrossRef](#)]